Available online at www.sciencedirect.com

SciVerse ScienceDirect

Ceramics International 39 (2013) 5219–5225

CERAMICS INTERNATIONAL

www.elsevier.com/locate/ceramint

Ultrasound assisted synthesis of Gd and Nd doped ceria electrolyte for solid oxide fuel cells

Hikmet Okkay[a,*], Mahmut Bayramoğlu[a], M.Faruk Öksüzömer[b]

[a]*Gebze Institute of Technology, Department of Chemical Engineering, 41400 Kocaeli, Turkey*
[b]*Istanbul University, Department of Chemical Engineering, Avcılar 34320, Istanbul, Turkey*

Received 25 September 2012; received in revised form 29 November 2012; accepted 7 December 2012
Available online 23 December 2012

Abstract

In this study, the ceramic powders of $Ce_{1-x}Gd_xO_{2-x/2}$ and $Ce_{1-x}Nd_xO_{2-x/2}$ (x=0.05, 0.10, 0.15, 0.20 and 0.25) were synthesized by ultrasound assisted co-precipitation method. The ionic conductivity was studied as a function of dopant concentration over the temperature range of 300–800 °C in air, using the impedance spectroscopy. The maximum ionic conductivity, $\sigma_{800\,^\circ C}=4.01\times10^{-2}$ Scm^{-1} with the activation energy, $E_a=0.828$ $kJmol^{-1}$ and $\sigma_{800\,^\circ C}=3.80\times10^{-2}$ Scm^{-1} with the activation energy, $E_a=0.838$ $kJmol^{-1}$ were obtained for $Ce_{0.90}Gd_{0.10}O_{1.95}$ and $Ce_{0.85}Nd_{0.15}O_{1.925}$ electrolytes, respectively. The average grain size was found to be in the range of 0.3–0.6 μm for gadolinium doped ceria and 0.2–0.4 μm for neodymium doped ceria. The uniformly fine crystallite sizes (average 12–13 nm) of the ultrasound assisted prepared powders enabled sintering of the samples into highly dense (over 95%) ceramic pellets at 1200 °C (5 °C min^{-1}) for 6 h.

Keywords: C. Ionic conductivity; Ultrasound; SOFC; Solid electrolyte

1. Introduction

Solid electrolyte has been considered as one of the most important parts affecting the performance of solid oxide fuel cell (SOFC). Rare-earth doped ceria has been regarded among the most promising electrolyte types due to high-conductivity and good-compatibility with electrodes for SOFCs in the intermediate-temperature range of 500–800 °C [1,2].

The ionic conductivity of rare-earth doped ceria systems depends mainly on the kind of dopant and its concentration, which is promoted by suitable trivalent additives such as Sm^{3+}, Gd^{3+} or Nd^{3+} [3,4]. However, reported results of maximum ionic conductivities versus dopant types and concentrations are generally contradictive. This disagreement probably results from divergences in sample preparation, amount of impurities in the material and oxygen ionic conductivity measurement methods [5,6]. Recently, Hui et al. [7] have discussed and reviewed the important parameters such as composition, microstructure and processing on the ionic conductivity improvements for oxide electrolytes. The microstructural parameters influencing the ionic conductivity depend mainly on the characteristics of the starting powders, which differs depending on the synthesis method and conditions used [8,9]. Generally, several synthesis methods have been employed to produce oxide electrolytes such as conventional solid state [10], sol–gel [6], hydrothermal [11], co-precipitation [12], and spray and freeze drying [5]. Chemical precipitation is a simple and feasible technique for synthesizing ultrafine ceramic powders with high sinterability. This method offers some advantages, such as simple and rapid preparation, direct and precise control of stoichiometry, homogeneity and purity [13,14].

The sonochemical method has been extensively used to generate novel materials with unusual properties [15]. The chemical and mechanical effects of ultrasound are due to the cavitation phenomena which produces bubbles during the rarefaction (negative pressure) period of sound waves. The eventual collapse of bubbles generates intense local temperatures (hot spots of ~5000 °C), extreme pressures

*Corresponding author. Tel.: +90 262 6052112; fax: +90 262 6052105.
E-mail address: hokkay@gyte.edu.tr (H. Okkay).

0272-8842/$ - see front matter © 2012 Elsevier Ltd and Techna Group S.r.l. All rights reserved.
http://dx.doi.org/10.1016/j.ceramint.2012.12.021

(~1000 atm) and rapid heating and cooling rates (above 10^{10} Ks^{-1}). These high heating and cooling rates hinder the organization and crystallization of the products. Furthermore the fast kinetics does not permit the nuclei growth. Due to these extreme conditions, ultrasonic irradiation has been successfully applied to prepare various nano-sized materials such as metals and metal oxides [16–19]. Recently, it has been reported that the sonochemical technique is a suitable route to produce CeO_2 powders [20–24]. However, there is no information on the ionic conductivity of rare-earth doped ceria powders produced by ultrasound assisted synthesis.

In this study, two types of doped ceria electrolyte namely, gadolinium doped ceria (GDC) and neodymium doped ceria (NDC) were prepared at various dopant concentrations by ultrasound assisted co-precipitation method. The results of a systematic study investigating the effects of dopant type and concentrations on various characteristics of the ceria samples such as the ionic conductivity, the lattice parameters, the activation energy, the microstructure and the density were reported.

2. Materials and methods

2.1. Sample preparation

The ceramic powders of $Ce_{1-x}Gd_xO_{2-x/2}$ (GDC) and $Ce_{1-x}Nd_xO_{2-x/2}$ (NDC) ($x=0.05$, 0.10, 0.15, 0.20 and 0.25) were synthesized by ultrasound assisted co-precipitation method using cerium (III) nitrate hexahydrate ($Ce(NO_3)_3 \cdot 6H_2O$, >99.0% Fluka), gadolinium (III) nitrate hexahydrate ($Gd(NO_3)_3 \cdot 6H_2O$, 99.9% Aldrich) and neodymium (III) nitrate hydrate ($Nd(NO_3)_3 \cdot xH_2O$, 99.99% Aldrich) as starting materials. Stoichiometric amounts of starting materials were dissolved separately in distilled water and mixed. The resulting solutions were then made up to 75 ml with water.

The hydrolysis reaction was conducted in a three neck round bottom flask equipped at the central neck with a horn type titanium probe of 19 mm tip diameter. A pH probe was placed at side neck to continuously monitor the pH during the reaction. Low frequency (20 kHz) ultrasound was generated by means of an ultrasonic generator (Bandelin, Type HD-2200). The electrical power supply to the generator was measured using a power meter. Furthermore, the ultrasound power absorbed by the reaction medium was calculated by the calorimetric method. During the reaction, the temperature of the solution was kept at room temperature (25 ± 2 °C). Experimental setup is shown in Fig. 1. For all experiments, the ultrasound power was adjusted as 15.0 ± 1.0 Wcm^{-2} acoustic intensity, using 19 mm probe and 8:2 pulse ratio.

For each synthesis, firstly the nitrate solution was poured into the reactor and then 4N NH_4OH solution was pumped until pH 9.5. During the hydrolysis reaction, the solution was sonicated for 30 min. At the end of the reaction, the precipitates were centrifuged, washed with distilled water and ethanol to remove the byproducts. After complete washing, the product was dried at 125 °C in an oven overnight. The same procedure was applied for conventional co-precipitation method without ultrasonic irradiation.

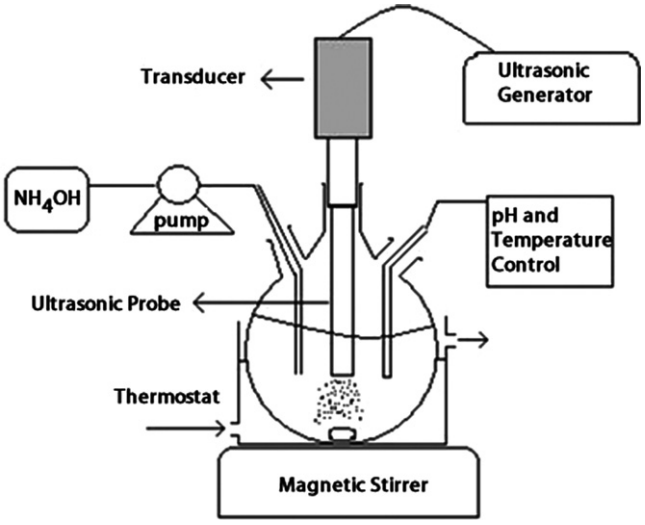

Fig. 1. Experimental setup for ultrasound assisted co-precipitation method.

The obtained powders were grounded and pressed into pellets, followed by cold-isostatic pressing at about 200 MPa. Subsequently, the samples were sintered at 1200 °C for 6 h with a programmed heating rate of 5 °C/min. The bulk densities of these sintered pellets were measured by the Archimedean method. The disk-shaped pellets with a thickness of around 1 mm and diameter of around 10 mm were used for the ionic conductivity measurement.

2.2. Characterization

Phase formation and crystal structure of the oxide powders were determined by X-ray diffraction (XRD) analysis. The X-ray spectra of rare-earth doped ceria powders were obtained over the 2θ range of 20–90° by using Bruker X-ray diffractometer with Cu-Kα radiation ($\lambda=0.15405$ nm) at a scanning rate of 4° min^{-1}. Calculation of the lattice parameters was carried out using four main reflections typical of a fluorite structure material with fcc (face-centered cubic) cell, corresponding to the (111), (200), (220) and (311) planes. The lattice parameters (a) of the GDC and NDC powders were calculated using the following relations;

$$d = \lambda/2\sin\theta \quad a = d\sqrt{(h^2+k^2+l^2)} \tag{1}$$

where d is the planar spacing, λ the wavelength of the radiation, θ the diffraction angle, and (a) is the lattice parameter. The average crystallite sizes of the oxide powders were calculated by the broadening of X-ray peak

performed on the (111), (200), (220) and (311) diffraction peaks using Scherer's equation.

The oxide ionic conductivities (σ) of the electrolytes were measured by electrochemical impedance spectroscopy based on the sintered pellets. Both sides of the pellets were coated with silver paste and then heated to 800 °C for 1 h before the measurement to ensure good bonding. The measurements of the oxygen conductivity were made by AC impedance analyzer (Solartron 1260 FRA and 1296 interface). The measurements were conducted in air in the frequency range from 0.05 Hz to 10 MHz and in the temperature range of 300–800 °C with an increment of 100 °C. Curve fitting and resistance calculation were done by ZView3.3a software. Total resistance of electrolyte is given by $R_t = R_b + R_{gb}$ where R_t, R_b and R_{gb} represent total resistance, bulk resistance and grain boundary resistance, respectively.

Then the conductivity was calculated using the equation; $\sigma = L/RS$ where L is the electrolyte thickness and S is the electrode area of the electrolyte surface. The activation energy for conduction is obtained by plotting the ionic conductivity data in the Arrhenius relation for thermally activated conduction. It was calculated according to the following equation;

$$\sigma \times T = \sigma_o \times \exp\left(-E_a/kT\right) \quad (2)$$

where E_a is the activation energy for conduction, T is the absolute temperature, σ_o is a pre-exponential factor, and k is Boltzmann's constant. The morphology and grain size of the sintered samples at 1200 °C were determined by scanning electron microscopy SEM Quanta FEG 450.

3. Results and discussion

The effects of dopant concentrations on the lattice parameter, the crystallite size, the relative density (%), the

Table 1
Lattice parameter, crystallite size, activation energy, % relative density and ionic conductivity of GDC and NDC at different concentration.

Sample	Ionic conductivity $\times 10^{-2}$ (Scm^{-1})	Lattice parameter (Å)	% of relative density	Activation energy ($kJmol^{-1}$)	Crystallite sizes (nm)
GDC05	2.420	5.4121	95.0	1.123	12.51
GDC10	4.010	5.4205	96.8	0.828	12.01
GDC15	3.560	5.4282	96.6	0.868	12.46
GDC20	3.259	5.4325	96.0	0.873	13.28
GDC25	3.190	5.4368	95.5	0.974	12.51
NDC05	1.834	5.4156	94.5	1.180	13.86
NDC10	2.390	5.4220	95.1	0.980	12.73
NDC15	3.808	5.4303	95.8	0.838	12.56
NDC20	3.423	5.4375	95.8	0.850	12.12
NDC25	2.957	5.4438	95.3	0.992	13.33

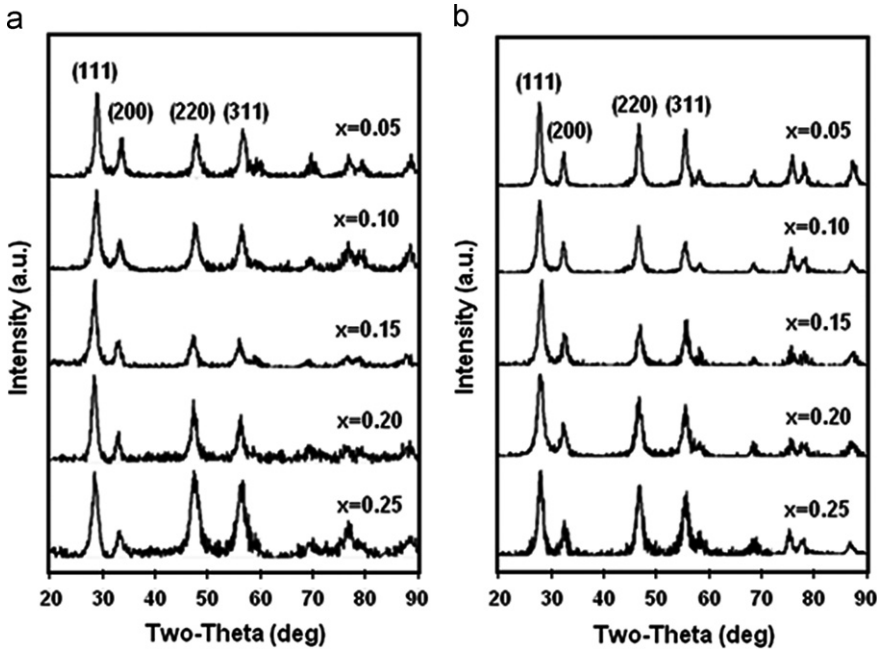

Fig. 2. Powder X-ray diffraction patterns of (a) GDC and (b) NDC nanocrystals synthesized by ultrasound assisted co-precipitation method.

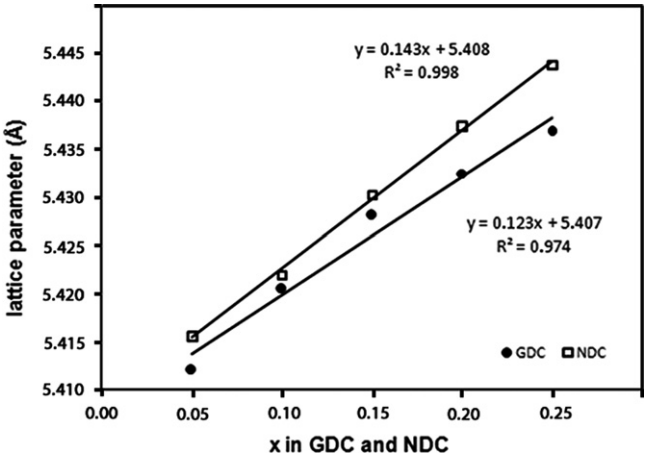

Fig. 3. Lattice parameters of GDC and NDC powders as function of dopant concentration.

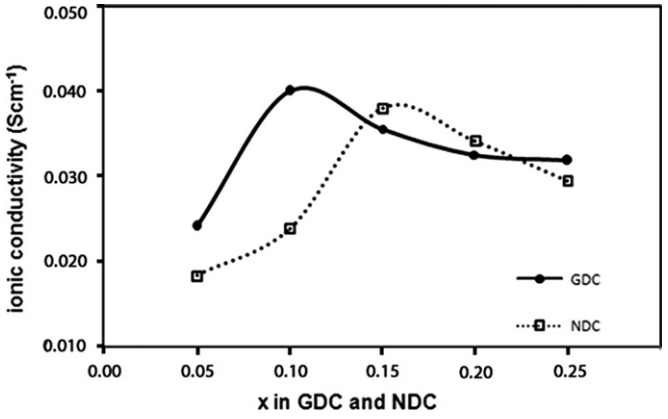

Fig. 4. Relationship between the dopant concentration and the ionic conductivity of GDC and NDC electrolytes at 800 °C.

activation energy as well as the ionic conductivity of the GDC and NDC samples are presented in Table 1.

The powder XRD patterns of as-prepared GDC and NDC nanocrystals are shown in Fig. 2. All the profiles were consistent with the cubic fluorite structure (Ref. JCPDS card 034-0394) expected of CeO_2. The average crystallite size of 12.5 nm and 13.0 nm GDC and NDC powders, respectively was obtained from the analysis of XRD measurements.

Fig. 3 shows the cubic lattice parameter of GDC and NDC crystals as a function of dopant concentration, for $x=0.05$–0.25. The lattice parameter increased with increasing gadolinium and neodymium content. As shown in Fig. 3, as the Nd and Gd content increases, the cubic lattice parameter increases linearly as $a(x)=5.408+0.143x$ for NDC powders and $a(x)=5.407+0.123x$ for GDC powders, respectively.

The relation between the dopant concentration and the ionic conductivity is shown in Fig. 4 which reveals that the ionic conductivities of GDC and NDC electrolytes are strongly related to the dopant concentration. In both cases, with increasing dopant concentration the conductivity increases until a maximum value, then it decreases with further increase in the dopant concentration. The occurrence of maximum points in these curves indicate the existence of conflicting causes which affect the ionic conductivity depending on the dopant concentration. By introducing increasing amount of dopant atoms in the ceria crystal, oxygen vacancy concentration increases and consequently the ionic conductivity increases. Furthermore, the formation of associations between dopants and oxygen vacancies at high dopant concentration causes a negative effect on the ionic conductivity [25].

The Arrhenius plots for the ionic conductivity of GDC and NDC electrolytes are shown in Fig. 5. As seen, the Arrhenius curves of both doped ceria electrolytes cannot be fitted by a single straight line. The curves show differing slopes, thus different activation energies, in the low and high temperature ranges. It is generally accepted that for

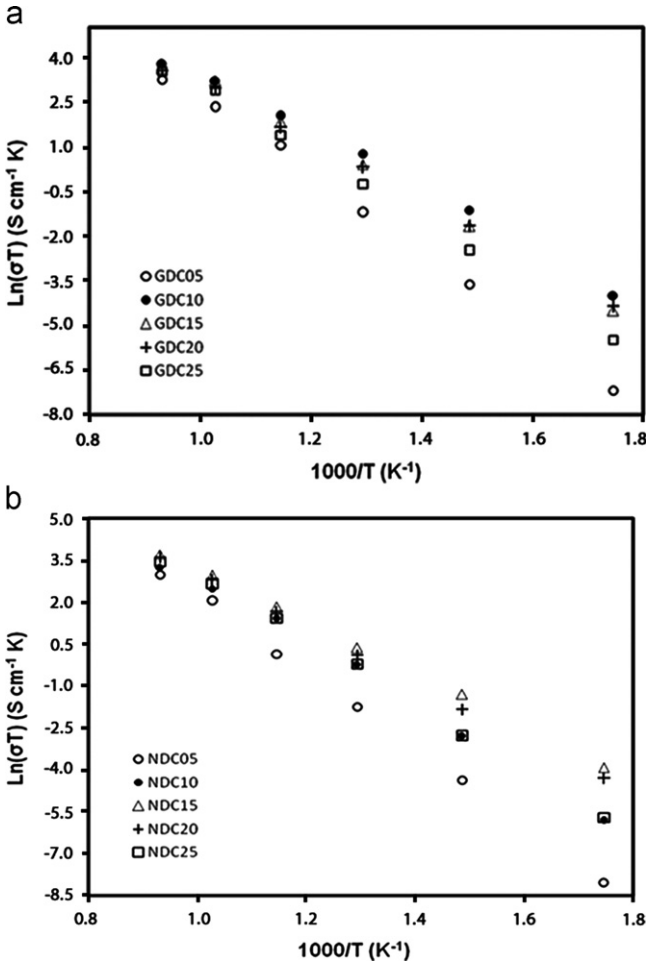

Fig. 5. The Arrhenius plot of the total conductivity of GDC (a) and NDC (b) electrolytes in air, synthesized by ultrasound assisted co-precipitation method.

oxygen diffusion in oxide electrolytes the activation energy is the sum of migration enthalpy for the oxygen ion and the association enthalpy of the local defect structure [26]. In the low temperature range (300–600 °C) where the association energy is important, the coulombic attractions

between defects with opposite charges lead to the formation of defect associates. On the other hand, at temperatures higher than 600 °C, the activation energy is specified dominantly by the migration enthalpy.

The variation of activation energy of GDC and NDC electrolytes in the temperature range of 300–800 °C as a function of dopant concentration is shown in Fig. 6. It is seen that both curves show similar behavior and the activation energy depending strongly on the dopant concentration. In the low dopant concentration range, the probability of formation of oxygen vacancy concentration increases and consequently the activation energy decreases. Meanwhile, further increase in the dopant concentration cause the association energy to be dominant on the activation energy. In conclusion, for GDC; the maximum ionic conductivity, $\sigma_{800\,^\circ C}=4.01\times10^{-2}\,Scm^{-1}$ with minimum activation energy, $E_a=0.828\,kJmol^{-1}$ occurred in the case of $Ce_{0.90}Gd_{0.10}O_{1.95}$ electrolyte. On the other hand, in the case of NDC; the maximum ionic conductivity, $\sigma_{800\,^\circ C}=3.80\times10^{-2}\,Scm^{-1}$ with the activation energy, $E_a=0.838\,kJmol^{-1}$ was obtained for $Ce_{0.85}Nd_{0.15}O_{1.925}$ electrolyte.

Table 2 summarizes the lattice parameter, crystallite size, activation energy, relative density and ionic conductivity of GDC and NDC electrolytes for two different methods. It is seen that lattice parameter and ionic conductivity of GDC and NDC electrolytes obtained by US method are much higher than that obtained by non-US method. Also, it should be noted that because of the lower crystallite size, the percentage of relative density obtained by US method are much higher than that obtained by non-US method. Similar results were reported earlier by Fu and Chen [12] for $Ce_{0.85}Nd_{0.15}O_{1.925}$ electrolyte prepared by co-precipitation method. They found that for NDC powders (20.1 nm crystallite size) sintered at 1500 °C for 5 h, the ionic conductivity $\sigma_{800\,^\circ C}=3.59\times10^{-2}\,Scm^{-1}$ with the activation energy, $E_a=0.820\,kJmol^{-1}$. However, similar results were obtained in this study for NDC at 1200 °C for 6 h sintering conditions.

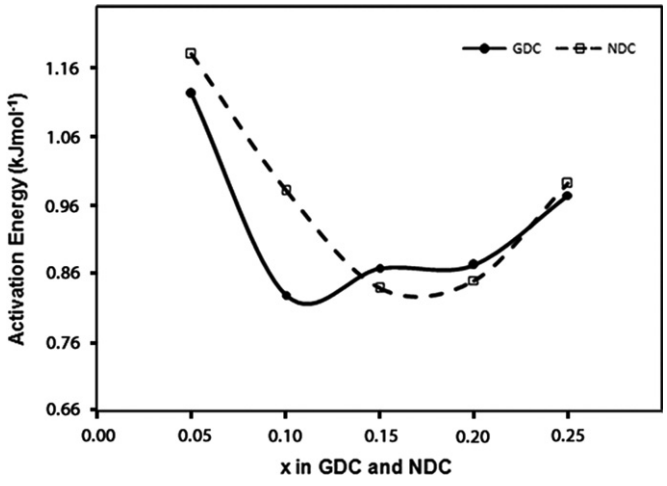

Fig. 6. Variation of activation energy as function of dopant concentration at 300–800 °C temperature ranges.

The microstructure of the sintered pellets of GDC and NDC were studied using SEM. Typical microstructures of GDC and NDC pellets are shown in Fig. 7a and b. It can be seen that the pellets indicate highly dense structure with formation of well-defined grain separated by grain boundary. The average grain size was found to be in the range of 0.3–0.6 μm for GDC and 0.2–0.4 μm for NDC, respectively.

It is known that the ceria electrolytes are difficult to densify below 1400 °C and nanocrytalline powders can provide faster densification kinetics and lower sintering temperatures [4,27]. In this work GDC and NDC powders were sintered to a relative density of over 95% at a lower sintering temperature of 1200 °C for 6 h. The lower sintering temperature provides important advantages such as reducing the cost and avoiding chemical interaction problems with electrodes. Another considerable advantage of ultrasound assisted co-precipitation method is the rapid preparation process to produce homogeneous and fine powders without the need for a calcination step.

4. Conclusions

The effect of the dopant type and concentration on ionic conductivities of the GDC and NDC electrolytes synthesized by ultrasound assisted co-precipitation method was studied. The ultrasound assisted co-precipitation method was shown to be an advantageous and efficient route to produce rare-earth doped ceria electrolytes. Also, fine powders of uniform crystallite sizes (average 12–13 nm) were obtained by this synthesis method. Because of the small particle size, the electrolyte powders could be sintered

Table 2
Comparative summary of GDC and NDC properties for both methods.

Sample	Ionic conductivity 10^{-2} (Scm^{-1})	Lattice parameter (Å)	% of relative density	Activation energy ($kJmol^{-1}$)	Crystallite sizes (nm)
GDC10[a]	2.590	5.4152	92.4	0.983	15.74
GDC10[b]	4.010	5.4205	96.8	0.828	12.01
NDC15[a]	2.502	5.4233	92.1	0.997	16.35
NDC15[b]	3.808	5.4303	95.8	0.838	12.56

[a]Conventional (non-US) co-precipitation method.
[b]Ultrasound assisted (US) co-precipitation method.

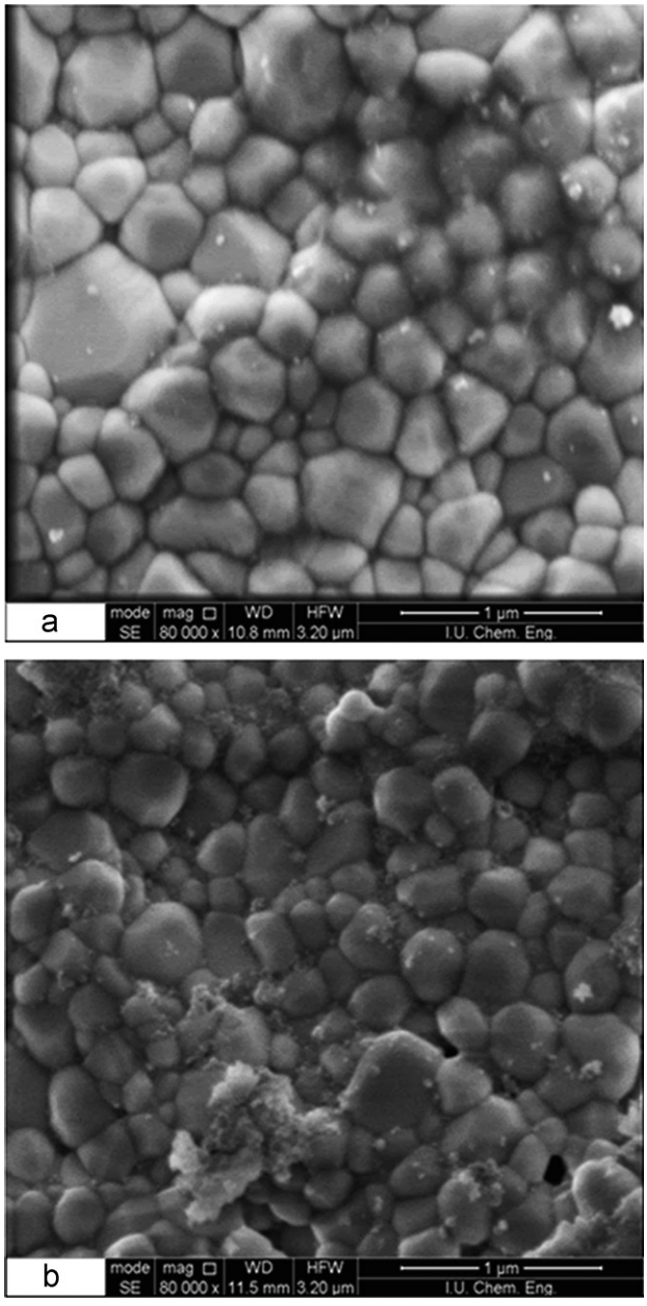

Fig. 7. SEM micrographs of electrolytes sintered at 1200 °C for 6 h. (a) GDC10 and (b) NDC15.

to a relative density of over 95% at a lower sintering temperature of 1200 °C for 6 h. This provides important advantages such as reducing the cost and avoiding chemical interaction problems with electrodes. For GDC the maximum ionic conductivity, $\sigma_{800\,^{\circ}C}=4.01\times10^{-2}\,Scm^{-1}$ with minimum activation energy, $E_a=0.828\,kJmol^{-1}$, occurred at $Ce_{0.90}Gd_{0.10}O_{1.95}$ electrolyte. The maximum ionic conductivity, $\sigma_{800\,^{\circ}C}=3.80\times10^{-2}\,Scm^{-1}$ with the activation energy, $E_a=0.838\,kJmol^{-1}$ was obtained for $Ce_{0.85}Nd_{0.15}O_{1.925}$ electrolyte. We conclude that the $Ce_{0.90}Gd_{0.10}O_{1.95}$ (GDC10) and the $Ce_{0.85}Nd_{0.15}O_{1.925}$ (NDC15) compositions are optimum for SOFC. The average grain size was found to be in the range of 0.3–0.6 μm for GDC and 0.2–0.4 μm for NDC.

References

[1] J.S. Ahn, S. Omar, H. Yoon, J.C. Nino, E.D. Wachman, Performance of anode-supported solid oxide fuel cell using novel ceria electrolyte, Journal of Power Sources 195 (2010) 2131–2135.
[2] T. Karaca, T.G. Altınçekiç, M.F. Öksüzömer, Synthesis of nanocrystalline samarium-doped CeO_2 (SDC) powders as a solid electrolyte by using a simple solvothermal route, Ceramics International 36 (2010) 1101–1107.
[3] Y.P. Fu, S.H. Chen, J.J. Huang, Preparation and characterization of $Ce_{0.8}M_{0.2}O_{2-y}$ (M = Y, Gd, Sm, Nd, La) solid electrolyte materials for solid oxide fuel cells, International Journal of Hydrogen Energy 35 (2010) 745–752.
[4] M. Chen, B.H. Kim, Q. Xu, B.K. Ahn, W.J. Kang, D.P. Huang, Synthesis and electrical properties of $Ce_{0.8}Sm_{0.2}O_{1.9}$ ceramics for IT-SOFC electrolytes by urea-combustion technique, Ceramics International 35 (2009) 1335–1343.
[5] J.C.C. Abrantes, D.P. Coll, P. Nunez, J.R. Frade, Electronic transport in $Ce_{0.8}Sm_{0.2}O_{1.9-\delta}$ ceramics under reducing conditions, Electrochimica Acta 48 (2003) 2761–2766.
[6] J.X. Zhu, D.F. Zhou, S.R. Guo, J.F. Ye, X.F. Hao, X.Q. Cao, J. Meng, Grain boundary conductivity of high purity neodymium-doped ceria nanosystem with and without the doping of molybdenum oxide, Journal of Power Sources 174 (2007) 114–123.
[7] S. Hui, J. Roller, S. Yick, X. Zhang, C.D. Petit, Y. Xie, R. Maric, D. Ghosh, A brief review of the ionic conductivity enhancement for selected oxide electrolytes, Journal of Power Sources 172 (2007) 493–502.
[8] A.L. Quinelato, E. Longo, E.R. Leite, M.I.B. Bernardi, J.A. Varela, Synthesis and sintering of ZrO_2–CeO_2 powder by use of polymeric precursor based on Pechini process, Journal of Materials Science 36 (2001) 3835-3830.
[9] K. Haberko, Characteristics and sintering behaviour of zirconia ultrafine powders, Ceramurgia International 5 (1979) 148–154.
[10] Y.J. Kang, G.M. Choi, The effect of alumina and Cu addition on the electrical properties and the SOFC performance of Gd-doped CeO_2 electrolyte, Solid State Ionics 180 (2009) 886–890.
[11] B. Rambabu, S. Ghosh, H. Jena, Novel wet-chemical synthesis and characterization of nanocrystalline CeO_2 and $Ce_{0.8}Gd_{0.2}O_{1.9}$ as solid electrolyte for intermediate temperature solid oxide fuel cell (IT-SOFC) applications, Journal of Materials Science 41 (2006) 7530–7536.
[12] Y.P. Fu, S.H. Chen, Preparation and characterization of neodymium-doped ceria electrolyte materials for solid oxide fuel cells, Ceramics International 36 (2010) 483–490.
[13] H. Li, C. Xia, M. Zhu, Z. Zhou, G. Meng, Reactive $Ce_{0.8}Sm_{0.2}O_{1.9}$ powder synthesized by carbonate coprecipitation: sintering and electrical characteristics, Acta Materialia 54 (2006) 721–727.
[14] R.O. Fuentes, R.T. Baker, Structural, morphological and electrical properties of $Gd_{0.1}Ce_{0.9}O_{1.95}$ prepared by a citrate complexation method, Journal of Power Sources 186 (2009) 268–277.
[15] K.S. Suslick, Ultrasound: Its Chemical, Physical and Biological Effects, VCH, Publishers, Weinheim, 1988.
[16] K.S. Suslick, G.J. Price, Applications of ultrasound to materials chemistry, Annual Review osf Materials Science 29 (1999) 295–326.
[17] A. Gedanken, Doping nanoparticles into polymers and ceramics using ultrasound radiation, Ultrasonics Sonochemistry 14 (2007) 418–430.
[18] K.S. Suslick, S.B. Choe, A.A. Cichowlas, M.W. Grinstaff, Sonochemical synthesis of amorphous ıron, Nature 353 (1991) 414–416.
[19] N.A. Dhas, A. Gedanken, Characterization of sonochemically prepared unsupported and silica-supported nanostructured pentavalent molybdenum oxide, Journal of Physical Chemistry B 101 (1997) 9495–9503.

[20] H. Wang, J.J. Zhu, J.M. Zhu, X.H. Liao, S. Xu, T. Ding, H.Y. Chen, Preparation of nanocrystalline ceria particles by sonochemical and microwave assisted heating methods, Physical Chemistry Chemical Physics 4 (2002) 3794–3799.
[21] M. Gasgnier, L. Albert, J. Derouet, L. Beaury, P. Maestro, T. Chopin, P. Caro, Ultrasound effects on cerium, praseodymium, and terbium oxides, Journal of Solid State Chemistry 112 (1994) 367–375.
[22] L. Yin, Y. Wang, G. Pang, Y. Koltypin, A. Gedanken, Sonochemical synthesis of cerium oxide nanoparticles-effets of additives and quantum size effect, Journal of Colloid and İnterface Science 246 (2002) 78–84.
[23] K. Niesz, D.E. Morse, Sonication-accelerated catalytic synthesis of oxide nanoparticles, Nano Today. 5 (2010) 99–105.
[24] D.V. Pinjari, A.B. Pandit, Room temperature synthesis of crystalline CeO_2 nanopowder: advantage of sonochemical method over conventional method, Ultrasonics Sonochemistry 18 (2011) 1118–1123.
[25] S. Yamazaki, T. Matsui, T. Ohashi, Y. Arita, Defect structures in doped CeO_2 studied by using XAFS spectrometry, Solid State Ionics 136 (2000) 913–920.
[26] S. Omar, E.D. Wachsman, J.L. Jones, J.C. Nino, Crystal structure-ionic conductivity relationships in doped ceria system, Journal of the American Ceramic Society 92 (2009) 2674–2681.
[27] X. Zhang, C.D. Petit, S. Yick, M. Robertson, O. Kesler, R. Maric, D. Ghosh, A study on sintering aids for $Sm_{0.2}Ce_{0.8}O_{1.9}$ electrolyte, Journal of Power Sources 162 (2006) 480–485.